



Cite this: RSC Adv., 2023, 13, 29163

Graphene quantum dots (GQD) and edge-functionalized GQDs as hole transport materials in perovskite solar cells for producing renewable energy: a DFT and TD-DFT study

 Anjan Kumar, ^a M. I. Sayyed, ^{bc} Diego Punina, ^d Eugenia Naranjo, ^e Edwin Jácome, ^f Maha Khalid Abdulameer, ^{*g} Hamza Jasim Albazoni ^h and Zahra Shariatinia ⁱ

This study investigated the potential suitability of graphene quantum dots (GQD) and certain edge-functionalized GQDs (GQD-3Xs) as hole transport materials (HTMs) in perovskite solar cells (PSCs). The criteria for appropriate HTMs were evaluated, including solubility, hole mobility, light harvesting efficiency (LHE), exciton binding energy (E_b), hole reorganization energy (λ_h), hole mobility, and HTM performance. It was found that several of the compounds had higher hole mobility than Spiro-OMeTAD, a commonly used HTM in PSCs. The open circuit voltage and fill factor of the suitable GQD and GQD-3Xs were found to be within appropriate ranges for HTM performance in MAPbI_3 PSCs. GQD-COOH and GQD-COOCH₃ were identified as the most suitable HTMs due to their high solubility, small λ_h , and appropriate performance.

 Received 10th August 2023
 Accepted 27th September 2023

 DOI: 10.1039/d3ra05438a
rsc.li/rsc-advances

Introduction

Hole transport materials (HTM) are of utmost importance in the optimization of perovskite solar cells (PSCs), which have garnered considerable interest from both scientists and industrial sectors owing to their remarkable characteristics like high efficiency, cost-effectiveness, and facile integration *via* roll-to-roll fabrication techniques.¹⁻³ The PSC has emerged as a transformative technology in the realm of photovoltaics, exhibiting a significant improvement in efficiency from 3.7% to 25.8% within a very short timeframe. This remarkable progress positions PSCs as a strong contender to conventional silicon solar cells.^{4,5} PSCs often have a light-absorbing layer positioned between the HTM and the electron transport material (ETM).

The primary function of the HTM is to assist in the extraction of holes while impeding charge recombination at the interface between the HTM and the perovskite layer.⁶ In order to be deemed appropriate for use in PSCs, HTMs must possess significant attributes like extraordinary hole transport capacity and conductivity, high mobility, a HOMO level that is well-aligned with the valence level of the perovskite material, favorable solubility to facilitate processability and cost-effectiveness.^{7,8} The effectiveness of a PSC device is significantly affected by the choice of HTMs since they fulfil many crucial functions. There are two primary functions of HTMs. Firstly, they serve to alter the energy barrier height that exists between the active layer and the electrode. Secondly, they create a specialized contact for the carriers. Furthermore, it is important to note that HTMs play a crucial role in providing a protective barrier, effectively safeguarding the active layer from any physical or chemical interactions that may arise between the electrode and the active layer. In addition, these entities play a crucial role in enhancing the process of charge transmission and collecting, hence contributing to the overall efficiency of the device. Finally, it should be noted that the use of HTMs has a remarkable role in enhancing the stability of both the active layer and the electrode. This aspect holds immense importance as it directly influences the overall stability of the device.^{4,8}

Spiro-OMeTAD, scientifically referred to as 2,2',7,7'-tetrakis-(*N,N*-di-*p*-methoxyphenylamine), the compound known as 9,9'-spirobifluorene has been more favored as a HTM in the advancement of PSCs. This is primarily attributed to its stable amorphous structure, capacity to generate thin films, and favorable electrical

^aDepartment of Electronics and Communication Engineering, GLA University, Mathura-281406, India

^bDepartment of Physics, Faculty of Science, Isra University, Amman 11622, Jordan

^cDepartment of Nuclear Medicine Research, Institute for Research and Medical Consultations (IRMC), Imam Abdulrahman bin Faisal University (IAU), PO Box 1982, Dammam, 31441, Saudi Arabia

^dFacultad de Ciencias de la Ingeniería, Carrera Ingeniería Mecánica, Universidad Técnica Estatal de Quevedo (UTEQ), Quevedo, Ecuador

^eFacultad Mecánica, Escuela Superior Politécnica de Chimborazo (ESPOCH), Riobamba, 060155, Ecuador

^fFacultad de Mecánica, Escuela Superior Politécnica de Chimborazo (ESPOCH), Riobamba, 060155, Ecuador

^gDepartment of Radiology & Sonar Techniques, Al-Noor University College, Nineveh, Iraq. E-mail: maha.khalid@alnoor.edu.iq

^hCollege of Nursing, National University of Science and Technology, Dhi Qar, Iraq

ⁱDepartment of Chemistry, Tehran Polytechnic, Amirkabir University of Technology, P.O. Box: 15875-4413, Tehran, Iran



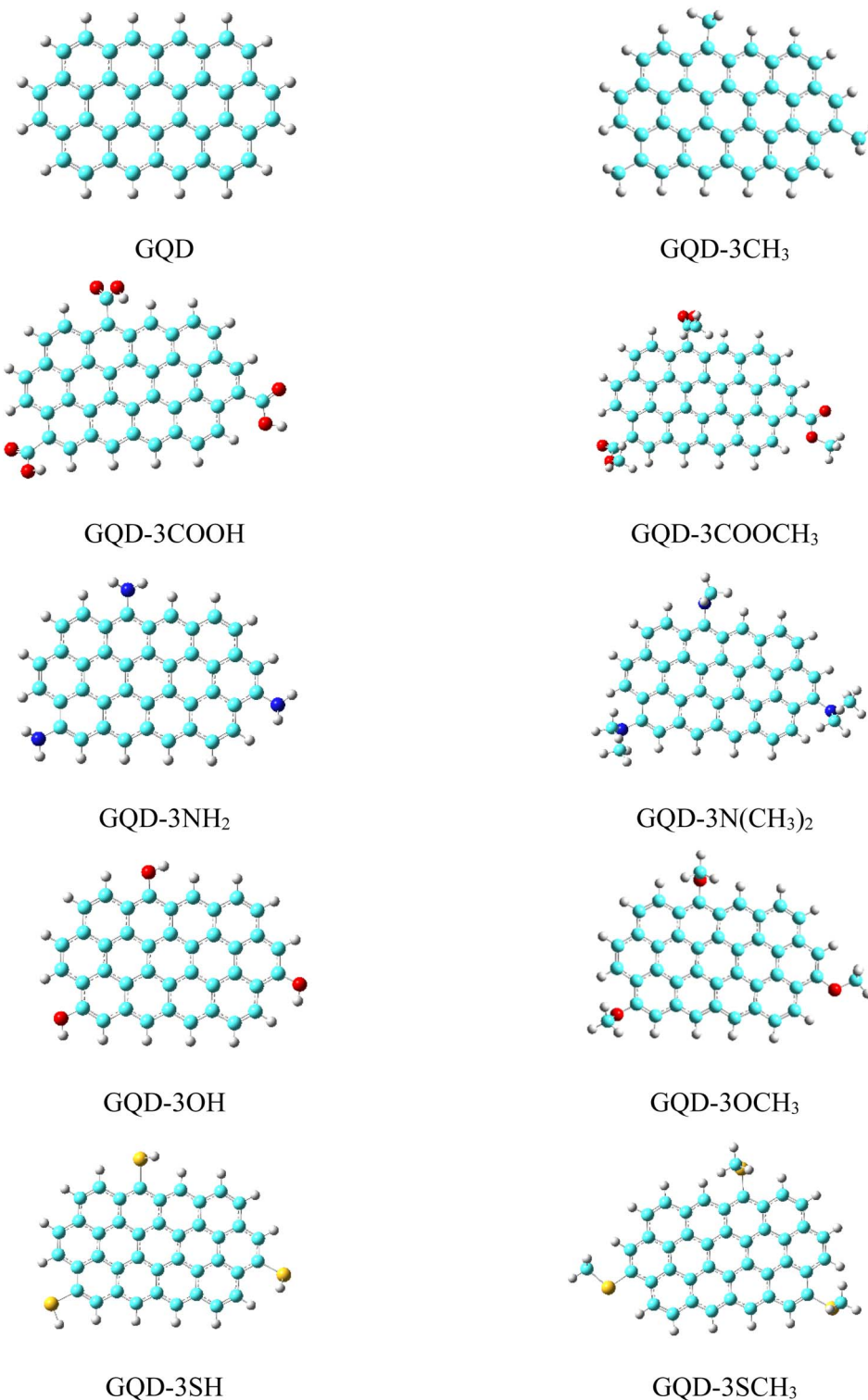


Fig. 1 The optimized geometries of the GQD and GQD-3Xs.

conductivity subsequent to doping.^{9–13} However, the high cost involved in its synthesis has prompted researchers to explore alternative materials.¹⁴ Fortunately, several simple and inexpensive alternatives for HTMs have been successfully developed, including fluorene,¹⁵ phenylamines,¹⁶ carbazole,^{17,18} furan,¹⁹ azine,²⁰ silolo-thiophene,²¹ and azomethine.²² Carbon quantum dots (CQDs)

have garnered significant interest in recent years owing to their distinctive characteristics and prospective uses as luminous nanomaterials.^{23–28} The first discovery of these entities occurred in 2004 by Xu *et al.* Subsequent investigations have been conducted to gain insights into their synthesis, characterisation, and prospective applications.^{27,29} CQDs are renowned for their



Table 1 Solvation energy ($\Delta E_{\text{solvation}}$), dipole momentum (D), and polarizability (α) of the GQD and GQD-3Xs

	$\Delta E_{\text{solvation}}$ (kcal mol ⁻¹)	D (gas phase) (Debye)	D (solvation) (Debye)	α (a.u.)
GQD	-4.70	0.00	0.00	832.03
GQD-3CH ₃	-4.88	0.13	0.28	900.55
GQD-3COOH	-14.43	6.20	9.16	935.27
GQD-3COOCH ₃	-12.92	6.78	9.05	976.71
GQD-3NH ₂	-11.68	3.46	4.51	919.62
GQD-3N(CH ₃) ₂	-5.51	1.26	1.87	1005.93
GQD-3OH	-9.65	1.67	2.22	867.20
GQD-3OCH ₃	-6.74	3.45	4.44	920.59
GQD-3SH	-6.72	1.78	2.50	968.79
GQD-3SCH ₃	-6.51	3.43	4.38	1022.86

remarkable stability and conductivity, little toxicity, and ecologically benign characteristics, making them very appealing for a different type of applications.^{27,28}

Graphene quantum dots (GQDs) have received most attention in contemporary discourse as a variant of CQDs. The GQDs are often characterized by their small dimensions, generally measuring less than 10 nanometers, and are mostly composed of carbon atoms.³⁰⁻³² However, it is possible to functionalize them in order to alter their features, such as adjusting the band gap, to cater to diverse applications. Carbon quantum dots (C-dots) are carbon atoms at the periphery of GQDs that have been fully saturated with hydrogen atoms.³³ C-dots have been the subject of substantial research due to their potential uses, notably in the field of photocatalysis. Numerous studies have shown the ability of carbon dots (C-dots) to function as exceptionally proficient photocatalysts, exhibiting remarkable catalytic efficacy. Furthermore, it has been shown that the boundaries of carbon dots (C-dots) possess the ability to impact the process of light absorption, hence emphasising its promising prospects in the field of photocatalysis.³⁴⁻³⁶

In recent times, there has been a growing attention in the use of CQDs, with a particular focus on GQDs, as highly efficient HTMs in the PSC. This interest stems from the remarkable attributes of CQDs, including their stability, non-toxic nature, cost-effectiveness, and environmentally friendly properties.³⁷⁻³⁹ A technique for producing nitrogen-functionalized graphene quantum dots (NGQDs) with adjustable optical properties was developed by Testsuka *et al.* Incorporating NGQD layers into optoelectronic devices, such as perovskite solar cells and hybrid phototransistors, significantly improved their performance.³⁷ Matta *et al.* employed density functional theory to examine a range of pristine and functionalized hexagonal GQDs and reported that GQDs functionalized with -OH and -COOH were effective for hole transport in MAPbI₃ as a PSCs.³⁸ Furthermore, Sorli *et al.* investigated the potential of 360 different coronene derivatives as small GQDs for hole transport, using both theoretical and experimental methods.³⁹ The present study aims to utilize DFT to examine the impact of the edge substitutions on the efficiency of GQDs as HTMs in perovskite solar cells.

This study investigates the potential of Graphene Quantum Dots (GQD) and a particular kind of edge-functionalized GQDs,

referred to as GQD-3Xs, as Hole Transport Materials (HTMs) with prospective applications in PSCs. The careful choice of suitable heterojunction materials (HTMs) plays a pivotal role in optimizing the overall performance of PSCs. In order to assess the appropriateness of these materials, a thorough set of criteria is used, including solubility, hole mobility, light harvesting efficiency (LHE), exciton binding energy (E_b), hole reorganization energy (λ_h), hole mobility, and hole transport material (HTM) performance. The method used in our study encompasses a series of methodical inquiries aimed at comprehensively characterizing the material characteristics and evaluating the performance of Graphene Quantum Dots (GQDs) and Triple-Doped Graphene Quantum Dots (GQD-3Xs) inside the framework of PSCs.

Computational details

The Berny optimization algorithm⁴⁰ was used to optimize the GQD and 9 functionalized GQDs. During the optimization process, we selected maximum force, RMS force, maximum displacement, and RMS displacement thresholds of 4.5×10^{-4} Hartree/Bohr, 3.0×10^{-4} , 1.8×10^{-3} Bohr, and 1.2×10^{-3} , respectively. The influence of dichloromethane solvent were studied by employing conductor-like polarizable continuum model (C-PCM) method.⁴¹ Imaginary frequencies were not found in the frequency calculations performed on pristine and functionalized GQDs. The UV-visible (UV-Vis) spectra were obtained using time-dependent density functional theory (TD-DFT) calculations.⁴² Natural bond orbitals analysis⁴³ accompanied with Chemcraft 1.7 (ref. 44) were employed to study and draw molecular orbitals of pristine and functionalized GQDs.

Eqn (1) and (2) were used to calculate the light harvesting efficiency (LHE) and exciton binding energy (E_b) of molecules considered GQDs.⁴⁵⁻⁴⁷

$$\text{LHE} = 1 - 10^{-f_{\text{max}}^{\text{abs}}} \quad (1)$$

$$E_b = E_g - E_{\text{opt}} \quad (2)$$

where, $f_{\text{max}}^{\text{abs}}$ is the oscillator strengths for the maximum absorption peak. E_g is defined as the gap energy between the HOMO and LUMO whereas E_{opt} is optical bandgap which is the gap energy between electronic ground state and first excited state.

All geometries were optimized using Grimme's dispersion corrected⁴⁸ B3LYP hybrid functional (B3LYP-D3) with 6-31G** basis sets through Gaussian 09 quantum package.⁴⁹ Also, B3LYP-D3 along with def2svp basis sets⁵⁰ were employed for NBO and TD-DFT calculations. B3LYP-D3/def2svp level of theory has been proved to simulate the electronic structures of CQDs and GQDs with reliable accuracy.³⁹

Results and discussion

Geometry, solubility, and dipole moment

The optimized geometries of the considered pristine and edge functionalized graphene quantum dots (GQD and GQD-3X,

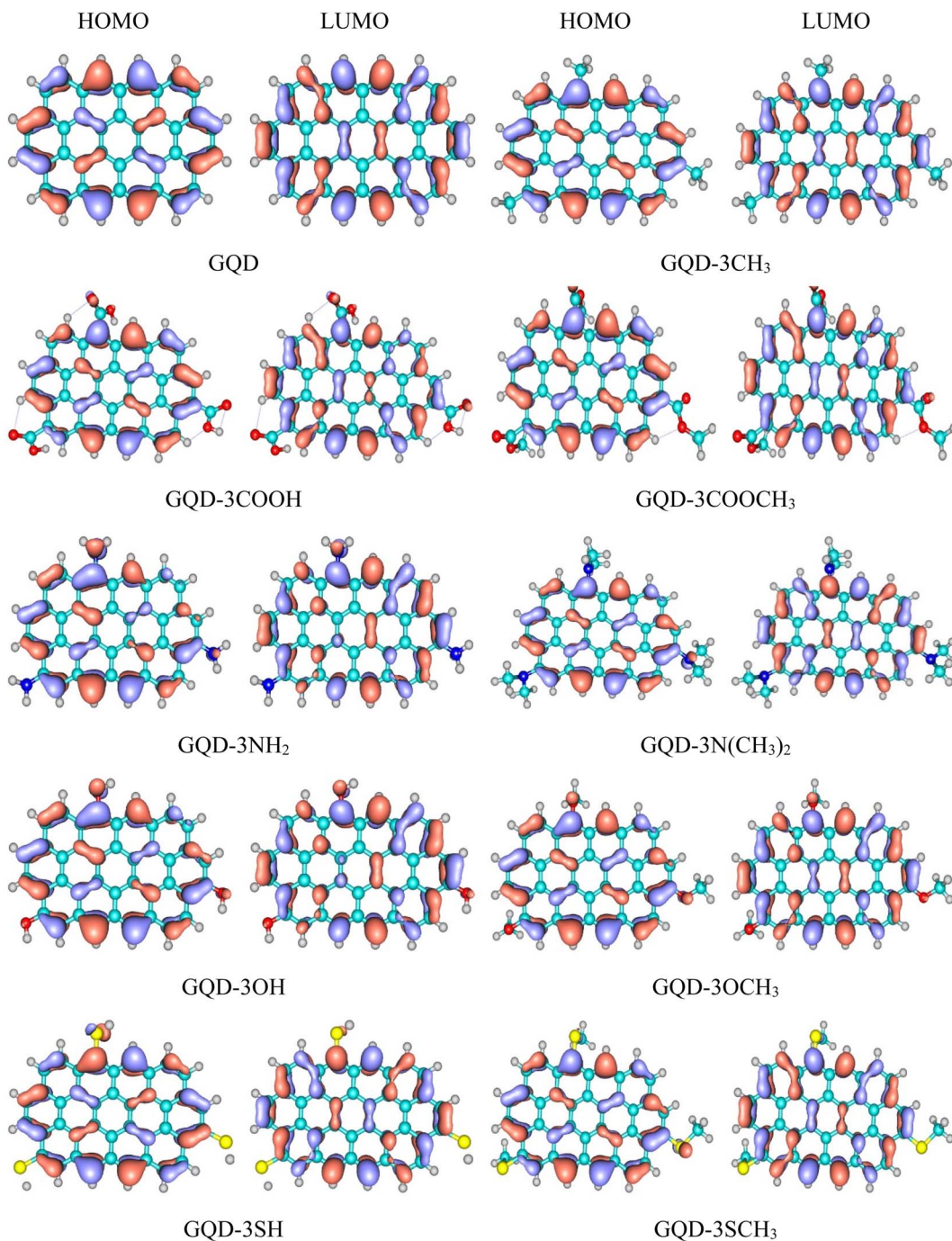


Fig. 2 The HOMO and LUMO schema of the GQD and GQD-3Xs.

$X = \text{CH}_3, \text{COOH}, \text{COOCH}_3, \text{NH}_2, \text{NMe}_2, \text{OH}, \text{OMe}, \text{SH}, \text{and SMe}$ in gas phase have been depicted in Fig. 1. In the development of organic electronic devices, solubility is a critical characteristic of HTMs. This term describes the capacity of a substance to dissolve in a specific solvent and form a homogenous solution. The significance of solubility lies in its impact on the ability to create a thin film of the material, which is a crucial element for the efficient performance of electronic devices.⁵¹ The formula $\Delta E_{\text{solvation}} = E_{\text{solution}} - E_{\text{gas}}$ was utilized to obtain the solvation energies of HTMs, where

E_{solution} and E_{gas} , respectively, represent the molecular energies in the solvent and gas phase.⁴⁷ The solvation energies of the GQD and GQD-3Xs in dichloromethane solvent have been imported in Table 1. The results indicate that the HTMs with the highest solvation energies are GQD-3COOH, GQD-3COOCH₃, and GQD-3NH₂, with values of $-14.45, -12.92$, and $-11.68 \text{ kcal mol}^{-1}$, respectively. These findings indicate that GQD-3COOH, GQD-3COOCH₃, and GQD-3NH₂ possess the greatest solubility among the HTMs considered. This phenomenon can be attributed to the strong hydrogen



Table 2 Calculated HOMO, LUMO, HOMO–LUMO gap (E_g), and Fermi energy (E_f) of the GQD and GQD-3Xs

	HOMO (eV)	LUMO (eV)	E_g (eV)	E_f (eV)
GQD	−4.96	−2.81	2.15	−3.88
GQD-3CH ₃	−4.88	−2.76	2.11	−3.82
GQD-3COOH	−5.30	−3.21	2.09	−4.25
GQD-3COOCH ₃	−5.23	−3.13	2.10	−4.18
GQD-3NH ₂	−4.55	−2.54	2.01	−3.55
GQD-3N(CH ₃) ₂	−4.82	−2.74	2.09	−3.78
GQD-3OH	−4.80	−2.71	2.09	−3.76
GQD-3OCH ₃	−4.86	−2.79	2.07	−3.82
GQD-3SH	−5.02	−2.96	2.06	−3.99
GQD-3SCH ₃	−5.00	−2.94	2.06	−3.97

bonding ability of the −COOH, −COOCH₃, and −NH₂ substituents with dichloromethane.

Table 1 also reports dipole moments of GQD and GQD-3Xs in gas phase and dichloromethane solvent. An inverse relationship exists between dipole moment and electron-carrier mobility. A high dipole moment indicates a low in electron-carrier mobility, while simultaneously improving the mobility of hole-carriers,⁵² improving organic electronic devices performance. GQD is a nonpolar compound due to its symmetric structure, which results in a lack of dipole moment. However, the introduction of edge functionalization can break its symmetry and enhance its dipole moment and polarity. Among the GQD-3Xs considered, GQD-3COOH and GQD-3COOCH₃ have the highest polarity, with dipole moments of 6.20 and 6.78 D in gas phase, respectively. Furthermore, dissolving GQD-3Xs in dichloromethane can increase their polarities.

Other factor which plays an significant role in the transport of charge carriers in materials, including hole transport materials used in organic electronic devices is polarizability.^{52,53} In the context of hole transport materials, polarizability can affect the mobility of charge carriers, including holes, within the material. Materials with high polarizability tend to have a higher interaction with electric fields, which can enhance the mobility of holes and improve the performance of devices such as organic solar cells. As seen in Table 1, the polarizability of GQD increases by replacing three edge hydrogens with selected substituents. Among these substituents, the highest polarizability is observed when hydrogens are replaced with the −S(CH₃) substituent.

Frontier orbital levels

The transportation of holes through a HTM is intricately connected to the energy levels of its HOMO and LUMO orbitals, which exert a profound influence on the overall efficacy of a PSC. The schemas of HOMO and LUMO of the considered GQD and GQD-3Xs in dichloromethane solvent have been illustrated in Fig. 2. Also, Table 2 reports the energies of HOMO and LUMO of the considered GQD and GQD-3Xs. To be suitable for PSC applications, a molecule must possess a HOMO level that is higher than that of the valence band (VB) the perovskite. MAPbI₃ (methylammonium lead iodide) is a perovskite material that has been widely studied for its potential use in solar cells.

Table 3 The main electronic configuration (MEC), wavelength (λ), oscillator strength (f), and the possibility of electronic configuration (P) of the first and the most intensive absorption lines of the GQD and GQD-3Xs. The H is HOMO and L is LUMO

Electronic excitation	λ (nm)	f	MEC	P
GQD				
S0 → S1	625.88	0.30	H → L	1.00
			H → L+2	0.51
GQD-3CH₃				
S0 → S1	637.48	0.31	H → L	1.00
			H → L+1	0.38
S0 → S6	388.96	1.96	H → L+2	0.24
			H → L+1	0.21
			H → L	0.12
			H → L+2	0.12
GQD-3COOH				
S0 → S1	646.75	0.29	H → L	1.00
			H → L+3	0.23
S0 → S6	401.43	1.44	H → L+2	0.21
			H → L+1	0.18
			H → L	0.14
			H → L+2	0.13
			H → L+1	0.11
GQD-3COOCH₃				
S0 → S1	643.75	0.30	H → L	1.00
			H → L+3	0.27
S0 → S6	398.75	1.40	H → L+2	0.23
			H → L+1	0.21
			H → L+2	0.13
			H → L+1	0.11
			H → L+2	0.11
GQD-3NH₂				
S0 → S1	680.33	0.27	H → L	1.00
			H → L+3	0.40
S0 → S7	408.32	0.89	H → L+2	0.29
			H → L+1	0.29
			H → L+2	0.11
			H → L+1	0.11
GQD-3N(CH₃)₂				
S0 → S1	649.89	0.29	H → L	1.00
			H → L+2	0.26
S0 → S7	416.82	0.89	H → L+2	0.22
			H → L+1	0.16
			H → L+2	0.14
			H → L+1	0.14
			H → L+2	0.13
GQD-3OH				
S0 → S1	650.45	0.27	H → L	1.00
			H → L+3	0.21
S0 → S7	394.31	1.36	H → L+2	0.18
			H → L+1	0.17
			H → L	0.15
			H → L+3	0.13
			H → L+1	0.13
			H → L+2	0.13
			H → L+1	0.13
GQD-3OCH₃				
S0 → S1	651.33	0.30	H → L	1.00
			H → L+2	0.43
S0 → S6	394.20	1.75	H → L+2	0.21
			H → L+1	0.21
			H → L	0.20
			H → L+2	0.20
GQD-3SH				
S0 → S1	655.08	0.32	H → L	1.00
			H → L+1	0.39
S0 → S6	405.18	1.54	H → L+2	0.19
			H → L	0.15
			H → L+3	0.15
			H → L+2	0.15



Table 3 (Contd.)

Electronic excitation	λ (nm)	f	MEC	P
			$H-1 \rightarrow L$	0.11
GQD-3SCH₃				
$S_0 \rightarrow S_1$	658.10	0.30	$H \rightarrow L$	1.00
$S_0 \rightarrow S_9$	376.76	0.91	$H-5 \rightarrow L$	0.68
			$H \rightarrow L+2$	0.12

The PSCs based on MAPbI₃ have shown high power conversion efficiency (PCE), which is a measure of how effectively the solar cell can convert light into electricity.^{54–56} The VB of MAPbI₃ was measured to be –5.43 eV.⁵⁷ As reported in Table 2, the HOMO energies of all GQD and GQD-3Xs are higher than HOMO level of MAPbI₃, indicating GQD and GQD-3Xs may be appropriate HTMs for MAPbI₃ based solar cells.

Another critical requirement for HTMs in PSC applications is their capacity to transport holes to the Au cathode. To fulfill this criterion, the HOMO level of the HTM should be situated below the Fermi level of the Au cathode, which is –5.1 eV.⁵⁸ As seen in Table 2, the HOMO energy levels of GQD-3COOH and GQD-3COOCH₃ are less than the Fermi level of Au cathode. An important observation to make is that, GQD-3COOH and GQD-3COOCH₃ possess HOMO energies that are more profound than Spiro-OMeTAD's HOMO energy of –5.20 eV.⁵⁹ As a result, it is plausible to anticipate that GQD-3COOH and GQD-3COOCH₃ are more suitable for use as HTMs compared to Spiro-OMeTAD.

In addition to proper position of HOMO, the LUMO level of a suitable HTM need to be located higher than the conduction band of MAPbI₃ perovskite (–3.93 eV).⁵⁷ Preventing the flow of photo-generated electrons from the MAPbI₃ layer back towards the Au electrode is the key reason for this requirement.⁴⁷ As observed in Table 1, the LUMO levels of all considered GQD and GQD-3Xs are positioned upper than the conduction band of MAPbI₃ perovskite.

UV-spectra and exciton binding energy

The UV-visible spectra for the GQD and GQD-3Xs were obtained using TD-DFT at the mentioned level. Table 3 provides the electronic configuration of the first and most intense absorption lines, while Fig. 3 displays the calculated UV-visible spectra with a half width at half height (HWHH) of 0.33 eV. The UV spectra of GQD and GQD-3Xs exhibit three significant peaks: a short peak in the 600–650 nm range, and two intense peaks in the 350–450 nm and 250–350 nm ranges. The short peaks are attributed to the $S_0 \rightarrow S_1$ electron excitation, which corresponds to electron excitation from HOMO to LUMO. The most intense absorption lines in the UV-visible spectra of GQD and GQD-3Xs, except for GQD-3NH₂, GQD-3N(CH₃)₂, GQD-3OH, and GQD-3SCH₃ are attributed to $S_0 \rightarrow S_6$ electron excitation. $S_0 \rightarrow S_7$ electron excitation accounts for the most intense absorption lines in GQD-3NH₂, GQD-3N(CH₃)₂, and GQD-3OH and $S_0 \rightarrow S_9$ corresponds to the most intensive absorption line in GQD-3SCH₃. Furthermore, the

light harvesting efficiencies (LHEs) of the GQD and GQD-3Xs using eqn (1) presented in Table 4 demonstrate their suitable light absorption capabilities. As seen, the most LHEs correspond to GQD and GQD-CH₃ with value of 0.99 while GQD-NH₂ and GQD-3N(CH₃)₂ have the least LHE with value of 0.87.

The required energy for $S_0 \rightarrow S_1$ excitation corresponds to optical bandgap (E_{opt}). As shown in eqn (2), the difference between E_g and E_{opt} is the exciton binding energy (E_b) which indicates the strength of the coulombic attraction between the excited electron and the hole.⁴⁶ A large exciton binding energy implies a strong electron–hole interaction, which can result in reduced charge separation efficiency and decreased device performance, particularly for solar cells, where efficient charge separation is critical for high power conversion efficiency. Conversely, a small exciton binding energy can indicate weak electron–hole interactions, facilitating efficient charge separation and transport, making the material more suitable for optoelectronic applications. The E_b of the GQD and GQD-3Xs were found to be within the range of 0.17 to 0.19 eV (Table 4), indicating weak electron–hole interactions and high charge transfer in these materials.

Hole reorganization energy and hole mobility

The hole reorganization energy (λ_h) is the energy change that occurs in a system when it undergoes structural relaxation following the loss of electrons.⁶⁰ λ_h is calculated by:

$$\lambda_h = (E_0^+ - E_+) + (E_+^0 - E_0) \quad (3)$$

E_0^+ and E_+ are the cationic energies of optimized neutral and cationic structures, respectively. Also, E_+^0 and E_0 denote the neutral energies of optimized cationic and neutral structures. Minimizing the λ_h is crucial for achieving high charge carrier mobility in organic semiconductors.⁶⁰ Table 5 presents a comparison of the λ_h values for GQD and GQD-3Xs. The table indicates that, with the exception of GQD-3N(CH₃)₂ and GQD-3NH₂, the λ_h values of GQD and GQD-3Xs are all less than λ_h values of Spiro-OMeTAD (163.31 meV (ref. 8, 47, 60 and 61)), suggesting that they may have a better mobility than Spiro-OMeTAD.

The most stable molecular structure pairs of GQD and GQD-3Xs, and the Einstein ration were used for modeling their hole mobility:⁶²

$$\mu = \frac{e}{K_B T} \frac{1}{2n} \sum_i r_i^2 k_{h,i} P_i \quad (4)$$

where e , K_B , and T indicate unit electronic charge, Boltzmann constant (8.61733034), and temperature (298 K), respectively. r_i is centroid to centroid distance. Also, $k_{h,i}$ and P_i are the hole hopping rate and hoping possibility, respectively, and are obtained employing following equations:⁶²

$$k_h = \frac{v_h^2}{\hbar} \sqrt{\frac{\pi}{\lambda_h K_B T}} \exp\left(-\frac{\lambda_h}{4K_B T}\right) \quad (5)$$

$$P_i = \frac{k_i}{\sum_i k_i} \quad (6)$$

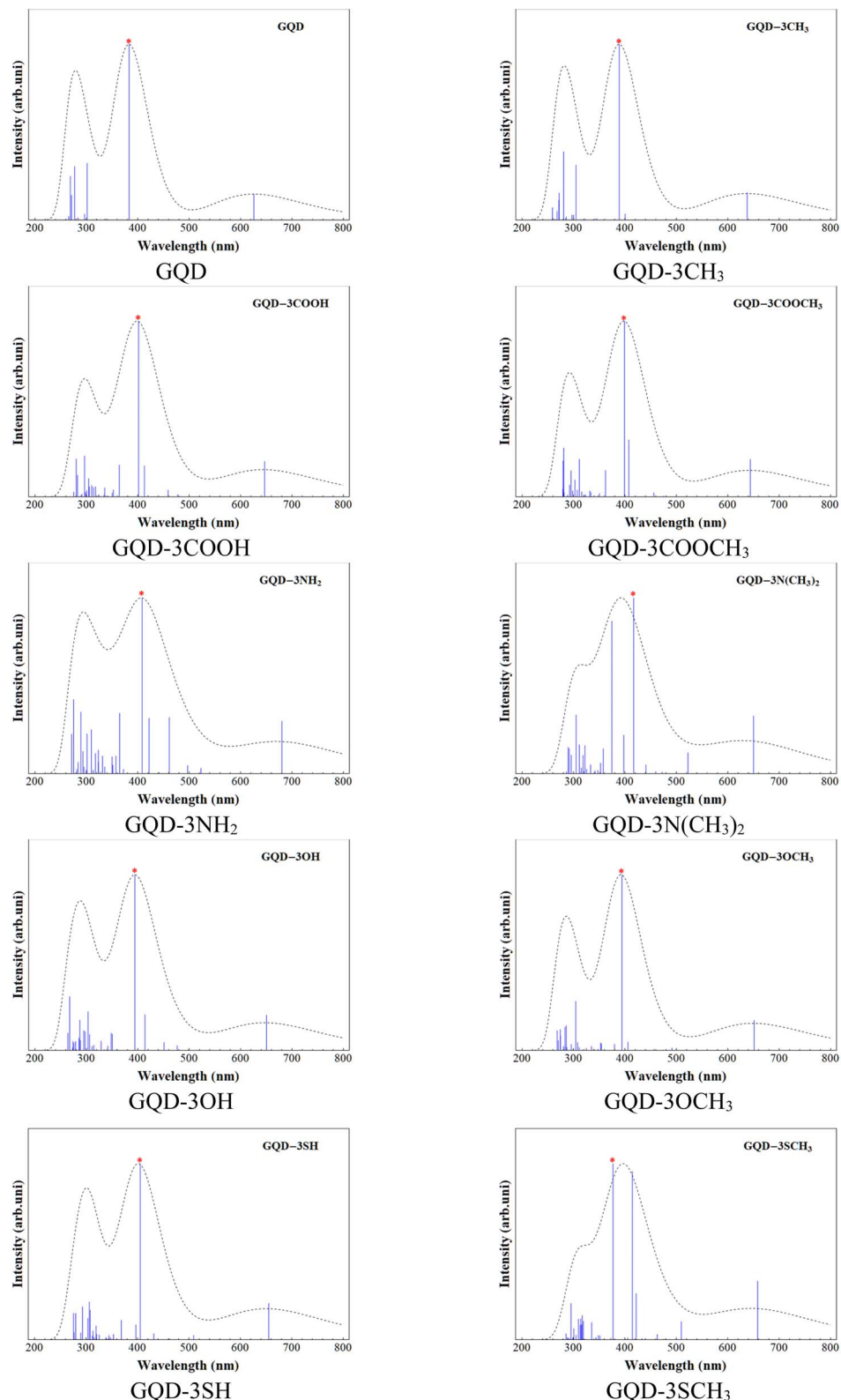


Fig. 3 The UV-visible spectra of the GQD and GQD-3Xs.

Table 4 HOMO–LUMO bandgap energy (E_g), optical bandgap energy (E_{opt}), oscillator strength of the most intensive absorption line (f_{max}), exciton binding energy (E_b), and light harvest efficiency (LHE) of the GQD and GQD-3Xs

	E_g (eV)	E_{opt} (eV)	f_{max}	E_b (eV)	LHE
GQD	2.15	1.98	1.99	0.17	0.99
GQD-3CH ₃	2.11	1.95	1.96	0.16	0.99
GQD-3COOH	2.09	1.92	1.44	0.17	0.96
GQD-3COOCH ₃	2.10	1.93	1.40	0.17	0.96
GQD-3NH ₂	2.01	1.82	0.89	0.19	0.87
GQD-3N(CH ₃) ₂	2.09	1.91	0.89	0.18	0.87
GQD-3OH	2.09	1.91	1.36	0.18	0.96
GQD-3OCH ₃	2.07	1.90	1.75	0.17	0.98
GQD-3SH	2.06	1.89	1.54	0.17	0.97
GQD-3SCH ₃	2.06	1.88	0.91	0.18	0.88

In eqn (5), ν_h is transfer integral and proximately obtained by:⁸

$$\nu_h = \frac{E_{\text{HOMO}}^{\text{pair}} - E_{\text{HOMO}-1}^{\text{pair}}}{2} \quad (7)$$

The hole mobility along with hole hopping rate, transfer integral, and centroid to centroid distance of the considered GQD and GQD-3Xs have been listed in Table 5. As seen, the hole mobility of all considered GQD and GQD-3Xs is more than

Table 5 Hole reorganization energy (λ_h), hole hopping rate (k_h), transfer integral (ν_h), centroid to centroid distance (r), hole mobility (μ), open circuit voltage (V_{OC}), and fill factor (FF) of the GQD and GQD-3Xs

	λ_h (meV)	k_h (s ⁻¹)	ν_h (eV)	r	μ (cm ² V ⁻¹ s ⁻¹)	V_{OC} (V)	FF
GQD	72.95	2.19×10^{14}	0.085	4.15	2.45	0.73	0.85
GQD-3CH ₃	77.13	1.17×10^{12}	0.0064	7.89	0.047	0.65	0.84
GQD-3COOH	100.04	1.15×10^{14}	0.076	3.45	0.89	1.07	0.89
GQD-3COOCH ₃	91.30	4.66×10^{12}	0.014	6.67	0.13	1.00	0.88
GQD-3NH ₂	196.80	9.17×10^{12}	0.041	5.85	0.20	0.32	0.74
GQD-3N(CH ₃) ₂	317.26	1.54×10^{13}	0.11	3.43	0.12	0.59	0.83
GQD-3OH	113.30	7.46×10^{12}	0.021	7.67	0.28	0.57	0.82
GQD-3OCH ₃	127.64	8.79×10^{12}	0.025	10.40	0.62	0.63	0.83
GQD-3SH	112.13	3.19×10^{11}	0.0044	9.89	0.020	0.79	0.86
GQD-3SCH ₃	79.95	1.31×10^{13}	0.022	11.40	1.10	0.77	0.86

Table 6 A summary for the comparison of GQD and GQD-3Xs in various criteria of HTMs

	H1 ^{a,d}	H2 ^{b,d}	L1 ^{c,d}	D (gas)	E_b	LHE	μ	V_{OC}	FF
GQD	0.47	-0.14	1.12	0.00	0.17	0.99	2.45	0.73	0.85
GQD-3CH ₃	0.55	-0.22	1.17	0.13	0.16	0.99	0.047	0.65	0.84
GQD-3COOH	0.13	0.20	0.72	6.20	0.17	0.96	0.89	1.07	0.89
GQD-3COOCH ₃	0.20	0.13	0.80	6.78	0.17	0.96	0.13	1.00	0.88
GQD-3NH ₂	0.88	-0.55	1.39	3.46	0.19	0.87	0.20	0.32	0.74
GQD-3N(CH ₃) ₂	0.61	-0.28	1.19	1.26	0.18	0.87	0.12	0.59	0.83
GQD-3OH	0.63	-0.30	1.22	1.67	0.18	0.96	0.28	0.57	0.82
GQD-3OCH ₃	0.57	-0.24	1.14		0.17	0.98	0.62	0.63	0.83
GQD-3SH	0.41	-0.08	0.97	1.78	0.17	0.97	0.020	0.79	0.86
GQD-3SCH ₃	0.43	-0.10	0.99	3.43	0.18	0.88	1.10	0.77	0.86
Spiro-OMeTAD	0.23	0.10	1.43	—	—	—	0.0057 (ref. 35)	0.97 ^e	0.88 ^e

^a $H1 = E_{\text{HOMO}}(\text{HTM}) - E_{\text{HOMO}}(\text{perovskite})$. ^b $H2 = E_{\text{Fermi}}(\text{Au}) - E_{\text{HOMO}}(\text{HTM})$. ^c $L1 = E_{\text{LUMO}}(\text{HTM}) - E_{\text{LUMO}}(\text{perovskite})$. ^d Negative sign indicates that the compound is not a suitable HTM. ^e Calculated by eqn (9) and (10).

calculated and experimental hole mobility values of Spiro-OMeTAD (2×10^{-4} to 6×10^{-3} cm² V⁻¹ s⁻¹).^{51,62,63} Among them, GQD, GQD-3SCH₃, and GQD-3COOH have the most hole mobility with values of 2.45, 1.10, and 0.89 cm² V⁻¹ s⁻¹, respectively.

Performances of PSCs

The performance of PSCs are proportional to their open circuit voltage (V_{OC}) and fill factor (FF) as described in following equation:⁶⁴

$$\text{PC} \propto V_{\text{OC}} \text{FF} \quad (8)$$

V_{OC} and FF can be calculated by eqn (6) and (7):⁶⁵

$$V_{\text{OC}} = (1/e)(E_{\text{LUMO}}(\text{acceptor}) - E_{\text{HOMO}}(\text{donor})) - 0.3 \text{ V} \quad (9)$$

In this case, MAPbI₃ perovskite is considered as acceptor and the GQD and GQD-3Xs are donors.

$$\text{FF} = \frac{\frac{e V_{\text{OC}}}{K_B T} - \ln\left(\frac{e V_{\text{OC}}}{K_B T} + 0.72\right)}{\frac{e V_{\text{OC}}}{K_B T} + 1} \quad (10)$$



Table 5 have been also reported V_{OC} and FF of the GQD and GQD-3Xs. As seen, the most values of V_{OC} are relative to GQD-3COOH, GQD-3COOCH₃, GQD-3SH, and GQD-3SCH₃ with values of 1.07, 1.00, 0.79, and 0.77 eV, respectively.

Table 6 presents a summary of the results obtained from evaluating various criteria for HTMs in the case of GQD and GQD-3Xs, and compares them to Spiro-OMeTAD. It is evident from the table that only GQD-3COOH and GQD-3COOCH₃ meet all the necessary criteria to be considered suitable HTMs. Additionally, these GQD-3Xs exhibit higher hole mobility and open circuit voltage compared to Spiro-OMeTAD. Consequently, GQD-3COOH and GQD-3COOCH₃ can be effectively utilized as efficient HTMs for perovskite solar cells.

Conclusion

In this study, the suitability of graphene quantum dot (GQD) and certain edge functionalized GQDs (GQD-3Xs, where X = CH₃, COOH, COOCH₃, NH₂, NMe₂, OH, OMe, SH, and SMe) as HTMs in PSCs was studied using DFT and TD-DFT. Specific criteria must be met for a compound to be considered an appropriate HTM in PSC, including the positioning of the HOMO of the HTM higher than the valence band (VB) of the perovskite, equal to or lower than the Fermi level of the gold cathode, and the LUMO energy level of the HTM higher than the conduction band (CB) of the perovskite. For this study, MAPbI₃ perovskite, which is widely used in PSCs, with VB and CB energy levels of -5.43 and -3.93 eV, respectively, was selected. Among the GQD and GQD-3Xs considered, the DFT calculations clarified that the HOMO levels of GQD and GQD-3Xs except for GQD-3COOH and GQD-3COOCH₃ were located higher than the Fermi level of Au cathode. As a result, these compounds do not meet the criteria, and they are not suitable as HTMs in PSC.

Solubility is a critical characteristic of HTMs in the development of organic electronic devices. The solubility of GQD and GQD-3Xs in dichloromethane was investigated in this study. It was found that GQD-COOH and GQD-COOCH₃ had the highest solubility, but these compounds did not meet the criteria to be used as suitable HTMs in PSCs. Among the compounds that met the criteria, GQD-3OH and GQD-3OCH₃ had the best solubility. The LHE and E_b of GQD and GQD-3Xs were determined by analyzing their UV-visible spectra. Among the compounds that met the criteria, their LHE was found to be greater than 0.87, indicating their potential for effective light harvesting. The calculated E_b values fell within the range of 0.17 to 0.19, suggesting their potential for efficient charge separation. The investigation of the hole reorganization energies (λ_h) and the hole mobility of GQD and GQD-3Xs revealed that the hole mobility of all compounds considered may be higher than Spiro-OMeTAD and other benzene derivatives commonly used as HTMs in PSCs. Additionally, the V_{OC} and fill factor (FF) of the GQD and GQD-3Xs that can be used as HTMs fall within the ranges of 0.57 to 1.07 V and 0.74 to 0.89, respectively, indicating their appropriate HTM performance in MAPbI₃ PSCs. Overall, due to its high solubility, small λ_h , and appropriate performance, GQD-COOH and GQD-COOCH₃ were found to be the

most suitable HTMs among the compounds considered in this study.

Conflicts of interest

The authors declare that they have no conflict of interest.

References

- Y. Rong, Y. Hu, A. Mei, H. Tan, M. I. Saidaminov, S. I. Seok, M. D. McGehee, E. H. Sargent and H. Han, Challenges for commercializing perovskite solar cells, *Science*, 2018, **361**, eaat8235.
- J.-P. Correa-Baena, M. Saliba, T. Buonassisi, M. Grätzel, A. Abate, W. Tress and A. Hagfeldt, Promises and challenges of perovskite solar cells, *Science*, 2017, **358**, 739–744.
- J. Y. Kim, J.-W. Lee, H. S. Jung, H. Shin and N.-G. Park, High-efficiency perovskite solar cells, *Chem. Rev.*, 2020, **120**, 7867–7918.
- S. Naqvi and A. Patra, Hole transport materials for perovskite solar cells: a computational study, *Mater. Chem. Phys.*, 2021, **258**, 123863.
- National Renewable Energy Laboratory, *Best research-cell efficiency chart*, NREL, 2023, <https://www.nrel.gov/pv/cell-efficiency.html>.
- C. Kou, S. Feng, H. Li, W. Li, D. Li, Q. Meng and Z. Bo, Molecular “flower” as the high-mobility hole-transport material for perovskite solar cells, *ACS Appl. Mater. Interfaces*, 2017, **9**, 43855–43860.
- M. Maciejczyk, A. Ivaturi and N. Robertson, SFX as a low-cost ‘Spiro’ hole-transport material for efficient perovskite solar cells, *J. Mater. Chem. A*, 2016, **4**, 4855–4863.
- N. S. Babu and I. O. Riwa, DFT and TD-DFT studies of 1,3,5-tris(diphenylamino)benzene derivatives based hole transport materials: application for perovskite solar cells, *Opt. Quantum Electron.*, 2022, **54**, 389.
- M. M. Lee, J. Teuscher, T. Miyasaka, T. N. Murakami and H. J. Snaith, Efficient hybrid solar cells based on meso-superstructured organometal halide perovskites, *Science*, 2012, **338**, 643–647.
- R. J. Westbrook, D. I. Sanchez-Molina, D. J. Manuel Marin-Beloqui, D. H. Bronstein and D. S. A. Haque, Effect of interfacial energetics on charge transfer from lead halide perovskite to organic hole conductors, *J. Phys. Chem. C*, 2018, **122**, 1326–1332.
- X. Zong, W. Qiao, Y. Chen, H. Wang, X. Liu, Z. Sun and S. Xue, New Efficient 1,1'-Bi-2-naphthylamine-Based Hole-Transporting Materials for Perovskite Solar Cells, *ChemistrySelect*, 2017, **2**, 4392–4397.
- H. Li, K. Fu, A. Hagfeldt, M. Grätzel, S. G. Mhaisalkar and A. C. Grimsdale, A simple 3,4-ethylenedioxythiophene based hole-transporting material for perovskite solar cells, *Angew. Chem.*, 2014, **126**, 4169–4172.
- N. J. Jeon, J. Lee, J. H. Noh, M. K. Nazeeruddin, M. Gratzel and S. I. Seok, Efficient inorganic–organic hybrid perovskite solar cells based on pyrene arylamine



derivatives as hole-transporting materials, *J. Am. Chem. Soc.*, 2013, **135**, 19087–19090.

14 J. Liang, L. Ying, W. Yang, J. Peng and Y. Cao, Improved efficiency of blue polymer light-emitting diodes using a hole transport material, *J. Mater. Chem. C*, 2017, **5**, 5096–5101.

15 Y. Hua, J. Zhang, B. Xu, P. Liu, M. Cheng, L. Kloo, E. M. Johansson, K. Sveinbjörnsson, K. Aitola and G. Boschloo, Facile synthesis of fluorene-based hole transport materials for highly efficient perovskite solar cells and solid-state dye-sensitized solar cells, *Nano Energy*, 2016, **26**, 108–113.

16 S. Park, J. H. Heo, C. H. Cheon, H. Kim, S. H. Im and H. J. Son, A [2,2]paracyclophane triarylamine-based hole-transporting material for high performance perovskite solar cells, *J. Mater. Chem. A*, 2015, **3**, 24215–24220.

17 S. Do Sung, M. S. Kang, I. T. Choi, H. M. Kim, H. Kim, M. Hong, H. K. Kim and W. I. Lee, 14.8% perovskite solar cells employing carbazole derivatives as hole transporting materials, *Chem. Commun.*, 2014, **50**, 14161–14163.

18 P. Gratia, A. Magomedov, T. Malinauskas, M. Daskeviciene, A. Abate, S. Ahmad, M. Grätzel, V. Getautis and M. K. Nazeeruddin, A methoxydiphenylamine-substituted carbazole twin derivative: an efficient hole-transporting material for perovskite solar cells, *Angew. Chem., Int. Ed.*, 2015, **54**, 11409–11413.

19 A. Krishna, D. Sabba, J. Yin, A. Bruno, P. P. Boix, Y. Gao, H. A. Dewi, G. G. Gurzadyan, C. Soci and S. G. Mhaisalkar, Facile Synthesis of a Furan–Arylamine Hole-Transporting Material for High-Efficiency, Mesoscopic Perovskite Solar Cells, *Chem.-Eur. J.*, 2015, **21**, 15113–15117.

20 M. Cheng, B. Xu, C. Chen, X. Yang, F. Zhang, Q. Tan, Y. Hua, L. Kloo and L. Sun, Phenoxazine-based small molecule material for efficient perovskite solar cells and bulk heterojunction organic solar cells, *Adv. Energy Mater.*, 2015, **5**, 1401720.

21 A. Abate, S. Paek, F. Giordano, J.-P. Correa-Baena, M. Saliba, P. Gao, T. Matsui, J. Ko, S. M. Zakeeruddin and K. H. Dahmen, Silolothiophene-linked triphenylamines as stable hole transporting materials for high efficiency perovskite solar cells, *Energy Environ. Sci.*, 2015, **8**, 2946–2953.

22 M. Petrus, T. Bein, T. Dingemans and P. Docampo, A low cost azomethine-based hole transporting material for perovskite photovoltaics, *J. Mater. Chem. A*, 2015, **3**, 12159–12162.

23 S. Y. Lim, W. Shen and Z. Gao, Carbon quantum dots and their applications, *Chem. Soc. Rev.*, 2015, **44**, 362–381.

24 R. Das, R. Bandyopadhyay and P. Pramanik, Carbon quantum dots from natural resource: a review, *Mater. Today Chem.*, 2018, **8**, 96–109.

25 L. Tian, Z. Li, P. Wang, X. Zhai, X. Wang and T. Li, Carbon quantum dots for advanced electrocatalysis, *J. Energy Chem.*, 2021, **55**, 279–294.

26 R. Jelinek, *Carbon quantum dots, carbon quantum dots*, Springer International Publishing, Cham, 2017, pp. 29–46.

27 Y. Wang and A. Hu, Carbon quantum dots: synthesis, properties and applications, *J. Mater. Chem. C*, 2014, **2**, 6921–6939.

28 R. Wang, K.-Q. Lu, Z.-R. Tang and Y.-J. Xu, Recent progress in carbon quantum dots: synthesis, properties and applications in photocatalysis, *J. Mater. Chem. A*, 2017, **5**, 3717–3734.

29 X. Xu, R. Ray, Y. Gu, H. J. Ploehn, L. Gearheart, K. Raker and W. A. Scrivens, Electrophoretic analysis and purification of fluorescent single-walled carbon nanotube fragments, *J. Am. Chem. Soc.*, 2004, **126**, 12736–12737.

30 Y. Yan, J. Chen, N. Li, J. Tian, K. Li, J. Jiang, J. Liu, Q. Tian and P. Chen, Systematic bandgap engineering of graphene quantum dots and applications for photocatalytic water splitting and CO₂ reduction, *ACS Nano*, 2018, **12**, 3523–3532.

31 M. Bacon, S. J. Bradley and T. Nann, Graphene quantum dots, *Part. Part. Syst. Charact.*, 2014, **31**, 415–428.

32 P. Tian, L. Tang, K. Teng and S. Lau, Graphene quantum dots from chemistry to applications, *Mater. Today Chem.*, 2018, **10**, 221–258.

33 G. Gao, Y. Jiao, F. Ma, Y. Jiao, E. Waclawik and A. Du, Carbon nanodot decorated graphitic carbon nitride: new insights into the enhanced photocatalytic water splitting from ab initio studies, *Phys. Chem. Chem. Phys.*, 2015, **17**, 31140–31144.

34 X. Feng, Y. Qin and Y. Liu, Size and edge dependence of two-photon absorption in rectangular graphene quantum dots, *Opt. Express*, 2018, **26**, 7132–7139.

35 H. Li, X. He, Z. Kang, H. Huang, Y. Liu, J. Liu, S. Lian, C. H. A. Tsang, X. Yang and S. T. Lee, Water-soluble fluorescent carbon quantum dots and photocatalyst design, *Angew. Chem., Int. Ed.*, 2010, **49**, 4430–4434.

36 J. Liu, Y. Liu, N. Liu, Y. Han, X. Zhang, H. Huang, Y. Lifshitz, S.-T. Lee, J. Zhong and Z. Kang, Metal-free efficient photocatalyst for stable visible water splitting via a two-electron pathway, *Science*, 2015, **347**, 970–974.

37 H. Tetsuka, A. Nagoya, T. Fukusumi and T. Matsui, Molecularly designed, nitrogen-functionalized graphene quantum dots for optoelectronic devices, *Adv. Mater.*, 2016, **28**, 4632–4638.

38 S. Kasi Matta, C. Zhang, A. P. O'Mullane and A. Du, Density functional theory investigation of carbon dots as hole-transport material in perovskite solar cells, *ChemPhysChem*, 2018, **19**, 3018–3023.

39 J. C. Sorli, P. Friederich, B. Sanchez-Lengeling, N. C. Davy, G. O. N. Ndjawa, H. L. Smith, X. Lin, S. A. Lopez, M. L. Ball and A. Kahn, Coronene derivatives for transparent organic photovoltaics through inverse materials design, *J. Mater. Chem. C*, 2021, **9**, 1310–1317.

40 H. B. Schlegel, Optimization of equilibrium geometries and transition structures, *J. Comput. Chem.*, 1982, **3**, 214–218.

41 B. Mennucci, Polarizable continuum model, *Wiley Interdiscip. Rev.: Comput. Mol. Sci.*, 2012, **2**, 386–404.

42 M. A. Marques and E. K. Gross, Time-dependent density functional theory, *Annu. Rev. Phys. Chem.*, 2004, **55**, 427–455.



43 F. Weinhold, Natural bond orbital analysis: a critical overview of relationships to alternative bonding perspectives, *J. Comput. Chem.*, 2012, **33**, 2363–2379.

44 *Chemcraft - graphical software for visualization of quantum chemistry computations*, <https://www.chemcraftprog.com>.

45 Y. Zhu, F. Zhao, W. Wang, Y. Li, S. Zhang and Y. Lin, Exciton Binding Energy of Non-Fullerene Electron Acceptors, *Adv. Energy Sustainability Res.*, 2022, **3**, 2100184.

46 J.-C. Lee, J.-D. Chai and S.-T. Lin, Assessment of density functional methods for exciton binding energies and related optoelectronic properties, *RSC Adv.*, 2015, **5**, 101370–101376.

47 Z. Shariatinia and S.-I. Sarmalek, Molecular engineering of several butterfly-shaped hole transport materials containing dibenzo[b,d]thiophene core for perovskite photovoltaics, *Sci. Rep.*, 2022, **12**, 13954.

48 S. Ehrlich, J. Moellmann, W. Reckien, T. Bredow and S. Grimme, System-Dependent Dispersion Coefficients for the DFT-D3 Treatment of Adsorption Processes on Ionic Surfaces, *ChemPhysChem*, 2011, **12**, 3414–3420.

49 M. J. Frisch, G. W. Trucks, H. B. Schlegel, G. E. Scuseria, M. A. Robb, J. R. Cheeseman, G. Scalmani, V. Barone, B. Mennucci, G. A. Petersson, H. Nakatsuji, M. Caricato, X. Li, H. P. Hratchian, A. F. Izmaylov, J. Bloino, G. Zheng, J. L. Sonnenberg, M. Hada, M. Ehara, K. Toyota, R. Fukuda, J. Hasegawa, M. Ishida, T. Nakajima, Y. Honda, O. Kitao, H. Nakai, T. Vreven, J. A. Montgomery Jr, J. E. Peralta, F. Ogliaro, M. Bearpark, J. J. Heyd, E. Brothers, K. N. Kudin, V. N. Staroverov, T. Keith, R. Kobayashi, J. Normand, K. Raghavachari, A. Rendell, J. C. Burant, S. S. Iyengar, J. Tomasi, M. Cossi, N. Rega, J. M. Millam, M. Klene, J. E. Knox, J. B. Cross, V. Bakken, C. Adamo, J. Jaramillo, R. Gomperts, R. E. Stratmann, O. Yazyev, A. J. Austin, R. Cammi, C. Pomelli, J. W. Ochterski, R. L. Martin, K. Morokuma, V. G. Zakrzewski, G. A. Voth, P. Salvador, J. J. Dannenberg, S. Dapprich, A. D. Daniels, O. Farkas, J. B. Foresman, J. V. Ortiz, J. Cioslowski and D. J. Fox, *Gaussian 09, Revision D.01*, Gaussian, Inc., Wallingford, CT, 2013.

50 F. Weigend, Accurate Coulomb-fitting basis sets for H to Rn, *Phys. Chem. Chem. Phys.*, 2006, **8**, 1057–1065.

51 S. S. Swayamprabha, M. R. Nagar, R. A. K. Yadav, S. Gull, D. K. Dubey and J.-H. Jou, Hole-transporting materials for organic light-emitting diodes: an overview, *J. Mater. Chem. C*, 2019, **7**, 7144–7158.

52 A. Tiwari, B. Kumar and A. K. Srivastava, Computational study on CH_3 -functionalized tetraphenyl-1,4-phenylenediamine: a hole-transporting material for OLED devices, *Mater. Today: Proc.*, 2020, **29**, 772–775.

53 W. Chen, S. Liu, Q. Li, Q. Cheng, B. He, Z. Hu, Y. Shen, H. Chen, G. Xu and X. Ou, High-Polarizability Organic Ferroelectric Materials Doping for Enhancing the Built-in Electric Field of Perovskite Solar Cells Realizing Efficiency over 24%, *Adv. Mater.*, 2022, **34**, 2110482.

54 Y. Raoui, H. Ez-Zahraouy, N. Tahiri, O. El Bounagui, S. Ahmad and S. Kazim, Performance analysis of MAPbI_3 based perovskite solar cells employing diverse charge selective contacts: simulation study, *Sol. Energy*, 2019, **193**, 948–955.

55 L. A. Frolova, A. I. Davlethanov, N. N. Dremova, I. Zhidkov, A. F. Akbulatov, E. Z. Kurmaev, S. M. Aldoshin, K. J. Stevenson and P. A. Troshin, Efficient and stable MAPbI_3 -based perovskite solar cells using polyvinylcarbazole passivation, *J. Phys. Chem. Lett.*, 2020, **11**, 6772–6778.

56 A. Y. Alsalloum, B. Turedi, X. Zheng, S. Mitra, A. A. Zhumekenov, K. J. Lee, P. Maity, I. Gereige, A. AlSaggaf and I. S. Roqan, Low-temperature crystallization enables 21.9% efficient single-crystal MAPbI_3 inverted perovskite solar cells, *ACS Energy Lett.*, 2020, **5**, 657–662.

57 P. Umari, E. Mosconi and F. De Angelis, Relativistic GW Calculations on $\text{CH}_3\text{NH}_3\text{PbI}_3$ and $\text{CH}_3\text{NH}_3\text{SnI}_3$ Perovskites for Solar Cell Applications, *Sci. Rep.*, 2014, **4**, 4467.

58 L. Caliò, S. Kazim, M. Grätzel and S. Ahmad, Hole-transport materials for perovskite solar cells, *Angew. Chem., Int. Ed.*, 2016, **55**, 14522–14545.

59 L. Nakka, Y. Cheng, A. G. Aberle and F. Lin, Analytical Review of Spiro-OMeTAD Hole Transport Materials: Paths toward Stable and Efficient Perovskite Solar Cells, *Adv. Energy Sustainability Res.*, 2022, **3**, 2200045.

60 M. Qiu, W. Pei, Q. Lu, Z. Li, Y. Li and J. Liang, DFT characteristics of charge transport in DBTP-based hole transport materials, *Appl. Sci.*, 2019, **9**, 2244.

61 J. D. Quezada-Borja, L. M. Rodríguez-Valdez, J. P. Palomares-Báez, M. A. Chávez-Rojo, L.-L. Landeros-Martínez, M. C. Martínez-Ceniceros, G. Rojas-George, I. A. García-Montoya and N. A. Sánchez-Bojorge, Design of new hole transport materials based on triphenylamine derivatives using different π -linkers for the application in perovskite solar cells. A theoretical study, *Front. Chem.*, 2022, **10**, 907556.

62 W.-J. Chi, Q.-S. Li and Z.-S. Li, Exploring the electrochemical properties of hole transport materials with spiro-cores for efficient perovskite solar cells from first-principles, *Nanoscale*, 2016, **8**, 6146–6154.

63 G. W. Kim, H. Choi, M. Kim, J. Lee, S. Y. Son and T. Park, Hole transport materials in conventional structural (n-i-p) perovskite solar cells: from past to the future, *Adv. Energy Mater.*, 2020, **10**, 1903403.

64 M. Afzal, N. Naeem, S. Iqbal, M. Al-Buriahi, N. Alfryyan, Z. Alrowaili and J. Iqbal, Rational design of dithieno[2,3-D:2',3'-D']benzo[1,2-B:4,5-B']dithiophene based small molecule donor for plausible performance organic solar cell, *Opt. Quantum Electron.*, 2023, **55**, 1–20.

65 M. C. Scharber, D. Mühlbacher, M. Koppe, P. Denk, C. Waldauf, A. J. Heeger and C. J. Brabec, Design rules for donors in bulk-heterojunction solar cells—towards 10% energy-conversion efficiency, *Adv. Mater.*, 2006, **18**, 789–794.

